Simulations of the melting of rare-gas inclusions in metals

1992 J. Phys.: Condens. Matter 4 5479

(http://iopscience.iop.org/0953-8984/4/25/004)

J. Phys.: Condens. Matter 4 (1992) 5479–5492. Printed in the UK

Simulations of the melting of rare-gas inclusions in metals

Michael Fearn, Kjeld O Jensen and Alison B Walker
School of Physics, University of East Anglia, Norwich NR4 7TJ, UK

Received 16 December 1991, in final form 8 April 1992

Abstract. Molecular dynamics simulations are reported of the melting of small inclusions of rare gases in cavities 10–20 Å in radius in metals containing a few hundred gas atoms. Such systems enable us to study the melting phenomena of clusters of atoms constrained by the cavity walls. We have looked at the positions of the atoms, the phase diagrams, and the importance of fluctuations for bubbles of different sizes. Melting in these systems takes place over a finite temperature range as in simulations of isolated clusters. The geometric structure factors have been calculated and compared with recent x-ray diffraction measurements of Andersen *et al* on krypton inclusions in aluminium. Our inability to reproduce the experimentally observed increase in the transverse diffraction peak width with temperature supports the suggestion of Andersen *et al* that this increase is due to a roughening transition of the aluminium facets of the cavities.

1. Introduction

A detailed understanding of melting is an outstanding challenge to condensed matter physicists. Although analytical approaches such as the recent one of Tallon [1] and computer simulations, e.g. those of Lee and Low [2], have made some headway, the process remains poorly understood. As far as computer simulation is concerned, the prime difficulty in looking at bulk melting lies in the need to simulate very large systems since the vacancy concentration at melting is about one in 10^4 atoms, and large systems are needed to make conclusions about the effects of defects such as vacancies [3], surfaces and interfaces [4].

However, it is possible to make some progress towards a theory of melting by studying small clusters of atoms which are easy to simulate and have a large surface to volume ratio, emphasizing surface contributions. Interest in phase transitions in finite systems has been spurred on by the observation of broadened solid–fluid transitions in simulations of isolated clusters [5, 6]. The melting transition for the clusters takes place over a finite temperature range as the temperature is raised, instead of at a well-defined melting temperature as for macroscopic systems [7–10]. Recent theoretical work [8–10] has indicated that in the transition region between the well-defined solid and fluid phases there is a phase coexistence between the solid and liquid phases with individual clusters at a given time being either all solid or all liquid. The fraction of clusters in a given phase changes with temperature which leads to the observation of a broadened transition when an ensemble of clusters is studied. Recent measurements of optical absorption spectra of benzene-doped Ar clusters [11] appear to be consistent with a coexistence region although this interpretation of the results has recently been questioned by Fried and Mukamel [12].

0953-8984/92/255479+14$04.50

An inherent difficulty in studying unsuspended clusters is the short time, i.e. the time of flight, over which the clusters can be observed. Much easier systems from an experimental point of view are rare-gas inclusions in metals, on which much work has been done in the last decade [13–25]. It is therefore important to establish if the phase transitions in the inclusions, in which the gas density, and hence the pressure, normally is very high, exhibit a broadening similar to that predicted for isolated clusters.

In this paper we report on molecular dynamics simulations of the melting of rare-gas inclusions. Our work was motivated by the experimental studies referred to above. Questions raised in those studies which we have tried to answer include: (i) whether a significant broadening of the melting transition is observed for typical bubble sizes and gas densities studied experimentally; (ii) whether the melting is initiated at the surface as suggested by Bohr [26]; (iii) the extent to which pressures differ from those predicted from a bulk equation of state.

We have also calculated the geometrical x-ray structure factors which enables a direct comparison to be made with the data reported in [13]. Our work follows on from simulations of noble-gas bubbles in metals by Jensen and Nieminen [27] who investigated the ordering of the rare-gas atoms at the interface. To our knowledge, the only other simulations which explicitly include the effect of the metal–rare-gas interactions in a cavity, those of Bug [28], were for systems with less than 50 atoms only and were confined to calculations of the pair correlation function and density. Chui [29] has studied particles, represented by hard spheres, in a spherical cavity by Monte Carlo simulations but made only indirect inferences about the melting process. These results are discussed in section 4.2 below, along with some very recent simulations of coated clusters by Broughton [30].

Rare-gas inclusions (bubbles) have attracted a great deal of technological interest, principally because they occur in radiation damage in fission and fusion reactors where neutrons produce He by (n, α) reactions within the reactor walls [31] and, in the case of the heavier rare gases, are used in ion beam modification of materials, e.g. the production of new alloys by ion beam mixing. Bubbles are likely to form in the bombarded materials because of the low solubility of rare gases in metals and the state of the particles, whether fluid or solid, will affect the growth of the inclusions both during implantation and subsequent annealing.

Our simulations have been made with parameters appropriate to krypton in aluminium to enable us to make direct comparisons with the measured x-ray scattering structure factors of Andersen *et al* [13]. These authors found from the x-ray diffraction peaks that their Kr-implanted Al samples contained a bi-modal distribution of bubbles with small bubbles of average radius 17.5 Å and large bubbles of average radius 90 Å. In this paper we concentrate on the behaviour of the smaller bubbles since these contain the highest density of gas and the effect of the cavity walls on the melting transition is expected to be more pronounced than for the large bubbles. In addition to 17.5 Å, we have also looked at bubble radii 14.4 Å and 10.0 Å, in order to establish how the bubble size affects the melting transition.

In section 2, we give the specifications of the system simulated and how the simulation was performed, including a discussion of how to calculate the pressure in a confined system and the geometrical x-ray structure factors. Section 3 covers our results and their implications are discussed in section 4. Section 5 summarizes our conclusions.

2. Methods

2.1. Cavity geometry

In these simulations the metal was taken as the continuum surroundings of a rigid cavity with smooth walls. The shape of the cavity is that of a body- centred-cubic Wigner–Seitz cell, namely a truncated octahedron bounded by ⟨111⟩ and ⟨100⟩ planes [32]. This shape is representative of a typical solid rare-gas bubble in a face-centred cubic metal [23]. The cavity can be considered as a cube of length L with its corners removed and has volume $L^3/2$. We determine L by setting the cavity volume equal to that of a spherical cavity with the effective radius required.

2.2. Metal–gas interactions

The metal–gas interaction potential was taken from the embedded atom approach of Manninen *et al* [33]. Here, the embedding energy of a rare-gas atom is calculated as a functional of the unperturbed electron density $n_0(r)$ of the metal, leading to a pairwise potential of the form

$$V(r) = \alpha n_0(r) \tag{1}$$

where α is a constant. By approximating $n_0(r)$ at the surface of the cavity by [34]

$$n_0(r) = n_{\text{bulk}}/(e^{r/\delta} + 1) \approx n_{\text{bulk}} e^{-r/\delta} \qquad r \gg \delta \tag{2}$$

where n_{bulk} is the bulk valence electron density and defining r as the distance along a normal to the cavity face, we obtain

$$V(r) = V_0 e^{-r/\delta}. \tag{3}$$

The force from a given face is assumed to be perpendicular to that face and the total force is found as the vector sum of the forces from all faces of the cavity surface. Values of α= 133 eV Å^3 [27] and δ=0.348 Å [34] were used. We have not included the weak attractive Van der Waals interaction discussed by Jensen and Nieminen [27] as it is not important at the high gas densities and small cavity sizes we have studied here. The embedded atom potential may not be particularly accurate for the heavier rare gases because of the large size of the atoms. However, the effect of the metal–gas potential is mainly to provide a rigid cavity in which the gas is contained and inaccuracies in the description of this potential will not affect our conclusions.

2.3. Gas–gas interactions

The Lennard-Jones 6–12 potential, i.e.

$$V(r) = 4\epsilon[(\sigma/r)^{12} - (\sigma/r)^6] \tag{4}$$

where r is the distance between two gas atoms, has been used for the gas–gas interactions since more accurate potentials, such as those of Siska *et al* [35] for Ne and Ross *et al* [36], are not very different from Lennard-Jones potentials [37] and not sufficiently different to affect the effects we are looking for. We have set ϵ/k_B = 164.0 K (where k_B is Boltzmann's constant) and σ=3.83 Å [38]. The potential was truncated at r=10 Å.

2.4. Simulation details

We have studied three sizes of cavities with effective radii R=10.0 Å, 14.4 Å and 17.5 Å containing 79, 201 and 459 atoms, repectively. The atoms were initially placed on a face-centred cubic lattice and given random velocities corresponding to the simulation temperature. The initial velocities were adjusted to make the linear and angular momenta equal to zero in the initial configuration. This procedure was used for the first run for each cavity size which was at room temperature. Subsequent runs were made at higher temperatures and used the positions and velocities from previous runs. This technique is a standard method for reducing equilibration times.

We calculated the trajectories of the rare-gas atoms using standard molecular dynamics methods for a fixed volume system as described, for example, in Allen and Tildesley [38]. A fifth-order predictor–corrector algorithm was used [38]. The timestep used was 5 fs and the temperature was rescaled every 30 timesteps. Although we use a constant-energy algorithm (i.e. solving Newton's equation of motion) the frequent temperature rescaling ensures that the simulations effectively take place at constant temperature [38] which is appropriate for clusters embedded in a metallic matrix held at a fixed temperature. The simulation code was checked by ensuring that it reproduced the pressure–volume isotherms of Kartunen *et al* [37] for bulk rare-gas solids.

For each bubble size, ten identical runs with different initial atomic velocities were done. The runs were done in parallel on a transputer array using job farming techniques. In each run the system was equilibrated first at 300 K after which the temperature was increased in 100 K steps. At each temperature the system was allowed to equilibrate for 5000 timesteps and subsequently followed for another 1000 timesteps to determine the physical quantities of interest.

The number of atoms and the exact value of the radius for the largest bubbles were adjusted to give a lattice parameter, as determined from the peaks in the structure factor, of 5.62 Å, close to the 5.55 Å measured in the experiments of Andersen *et al* [13]. The radii and number of particles for the small and medium-sized cavities was determined by the requirement that the pressure should be the same for all three sizes of cavity at room temperature which also implies that the lattice parameters are nearly identical for all bubbles sizes.

For comparison with the bubble simulations a bulk Kr simulation with 256 atoms at constant volume with periodic boundary conditions in all three dimensions was also performed. The density was adjusted to give the same pressure at 300 K as in the bubble simulations.

2.5. Pressure calculations

We have elected in this paper to calculate the pressure directly as the force exerted by the particles on the cavity walls per unit area. Denoting this pressure by P_{wall} we thus have

$$P_{\text{wall}} = \left\langle \frac{1}{A} \sum_{i=1}^{N} F_i^{\text{ext}} \right\rangle \tag{5}$$

where $\langle\ \rangle$ denotes a time average, A is the total surface area of the cavity and F_i^{ext} is the magnitude of the normal component of the force due to the wall on particle number i.

It is important to note that in the systems studied here this definition gives a pressure significantly different from that calculated using the method conventionally used in molecular dynamics simulations which uses the virial theorem. This pressure, P_{virial}, for a system of N particles at a temperature T in a volume Ω is [39]

$$P_{\text{virial}} = \frac{Nk_{\text{B}}T}{\Omega} + \langle W_{\text{int}} \rangle \tag{6}$$

where the internal virial W_{int} is given by

$$W_{\text{int}} = \frac{1}{3\Omega} \sum_{i=1}^{N} \boldsymbol{r}_i \cdot \boldsymbol{F}_i^{\text{int}}. \tag{7}$$

Here $\boldsymbol{F}_i^{\text{int}}$ is the force on the ith atom at $\boldsymbol{r}_i$ due to all other particles but excluding the forces $\boldsymbol{F}_i^{\text{ext}}$ due to the wall of the container. Equation (6) is obtained from the virial theorem which states that (see e.g. [40])

$$-\langle W_{\text{ext}} \rangle = \langle W_{\text{int}} \rangle + \frac{Nk_{\text{B}}T}{\Omega}. \tag{8}$$

where the external virial W_{ext} is defined as

$$W_{\text{ext}} = \frac{1}{3\Omega} \sum_{i=1}^{N} \boldsymbol{r}_i \cdot \boldsymbol{F}_i^{\text{ext}} \tag{9}$$

and by identifying $-W_{\text{ext}}$ with the pressure P_{virial}.

The discrepancy between P_{wall} and P_{virial} arises because of the range of the particle–wall forces not being vanishingly small compared to the total size of the system. This can be easily seen for a spherical cavity where $W_{\text{ext}} = (1/3\Omega)\sum_{i=1}^{N} r_i F_i^{\text{ext}}$ with r_i being the distance from the centre of the cavity. Since all r_i are smaller than or equal to the system radius R and $3\Omega = AR$ it follows that

$$P_{\text{wall}} \geqslant P_{\text{virial}}. \tag{10}$$

The equality in equation (10) holds when the wall force is of zero range (i.e. for a hard wall) since in this case F_i^{ext} is only different from zero when $r_i = R$.

We suspect that the inequality (10) holds for a cavity of general shape and certainly expect it to be valid in the present case, since the cavities are close to spherical. This is, in fact, confirmed by the results in section 3.2 below.

Powles *et al* [39] have also discussed the application of the virial theorem to pressure calculations in finite spherical systems. Their main result is that the virial pressure calculated for a subset of particles in the system may not correspond to the true pressure. However, since they consider a hard-walled container they find that what we term the wall and virial pressures are indeed identical when all particles of the system are included in the calculation of the internal virial. Their results are thus consistent with the discussion above.

2.6. X-ray structure factors

The x-ray intensity I for a scattering wavevector $\Delta k = k - k'$, where k, k' are, respectively, the incident and scattered x-ray wavevectors, is given by the modulus squared of the geometric structure factor [32]:

$$I = \frac{1}{N}\left|\sum_{i=1}^{N} e^{i\Delta k \cdot r_i}\right|^2 . \tag{11}$$

Here the sum is over the N rare-gas atoms in the cavity.

At the (111) peak

$$\Delta k = \frac{2\pi}{a_{Kr}}(1,1,1) \tag{12}$$

while for a radial scan

$$\Delta k = \frac{2\pi}{a_{Kr}}(1,1,1) + \frac{\delta_1}{\sqrt{3}}(1,1,1) \tag{13}$$

and for a transverse scan

$$\Delta k = \frac{2\pi}{a_{Kr}}(1,1,1) + \frac{\delta_2}{\sqrt{2}}(1,-1,0) \tag{14}$$

where a_{Kr} is the lattice constant of the Kr in the cavity and δ_1 and δ_2 are respectively the magnitudes of the deviation of the scattering wavevector from the scattering wavevector at the (111) peak for radial and transverse scans.

The geometry is shown in figure 1.

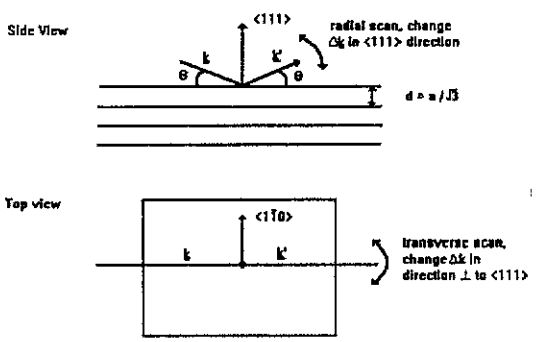

Figure 1. Schematic illustration of the geometry defining radial and transverse diffraction scans. Here k is the incoming x-ray wavevector, k' the outgoing x-ray wavevector, $\Delta k = k - k'$ is the scattering wavevector, and d the distance between adjacent lattice planes for a lattice of lattice constant a.

3. Results

3.1. Time-averaged particle positions

Figure 2 shows the positions of the gas particles from one of the simulation runs for cavities of effective radius 14.4 Å projected onto the ⟨100⟩ plane. The positions are shown for increasing temperatures of 300, 900, 1100 and 1300 K, in all cases averaged over 1000 timesteps. From the figure, it is clear that melting takes place between 1100 K and 1300 K. It is interesting to see that there is no evidence for premelting taking place at the surface of the inclusion. The melting would rather appear to be initiated at the corners, where the packing is less dense.

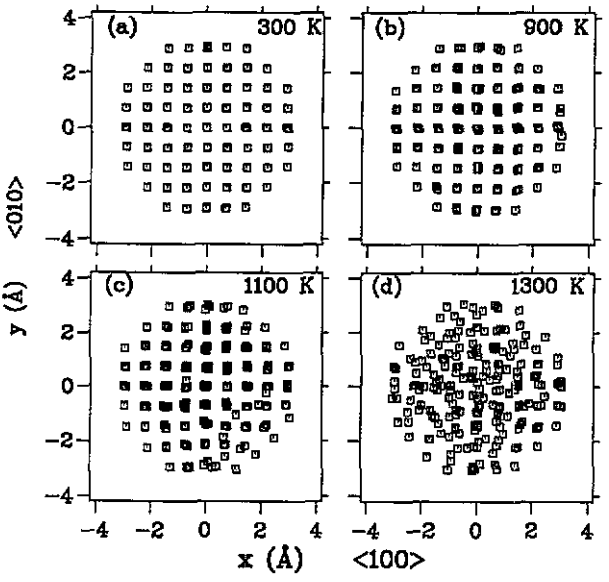

Figure 2. The positions of the 201 rare-gas atoms in a medium-size cavity (of effective radius 14.4 Å), projected onto the ⟨100⟩ plane for temperatures of 300 K (panel a), 900 K (panel b), 1100 K (panel c) and 1300 K (panel d).

3.2. Cavity pressures

Figure 3 shows the wall pressure, P_{wall}, and the virial pressure, P_{virial}, for cavities of effective radius 17.5 Å at increasing temperatures from 300 K to 1200 K. In all cases, the result shown is the average of the ten parallel simulations described in section 2.4. It is clear that the inequality (10) proven above holds and the approximately constant ratio between the two pressures is consistent with the fact that the inequality arises from the wall forces having a non-zero range.

The step in pressure between 700 and 800 K in figure 3 is associated with melting of the krypton as was confirmed by examining the atomic positions. The pressure results for all three bubble sizes and for the bulk system are shown in figure 4, again averaged over the ten simulation runs for each bubble size. In all systems a temperature range, in which melting takes place, can be identified, below and above

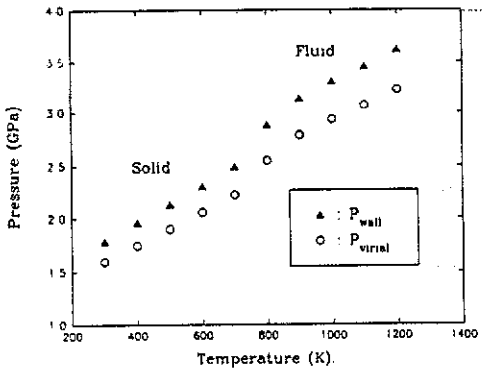

Figure 3. The wall pressure P_{wall} and virial pressure P_{virial} for cavities of effective radius 17.5 Å as functions of temperature.

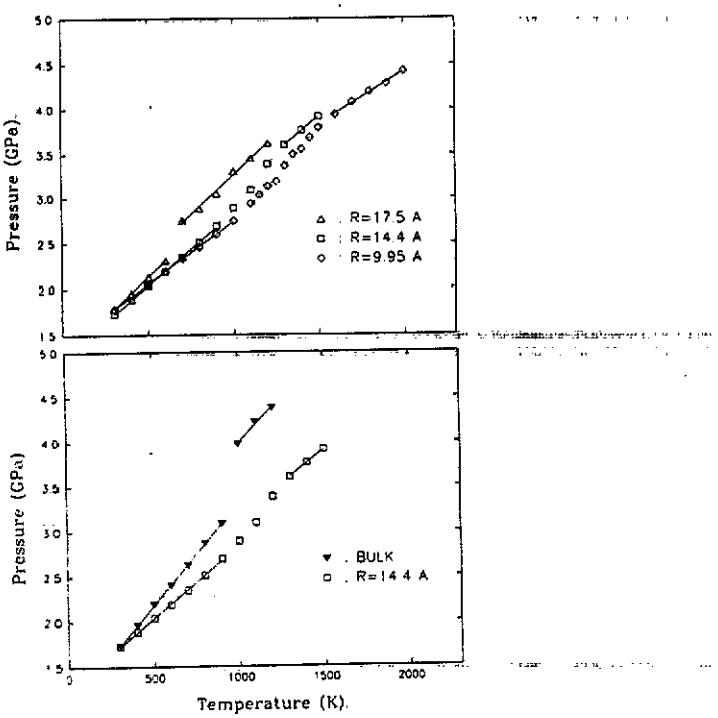

Figure 4. The wall pressure as a function of temperature for the small, medium and large cavities (panel a) and the medium-sized cavities compared to a bulk system of the same density (panel b).

which the pressure varies linearly with temperature. This is in accordance with the observations for isolated clusters [8, 10]. We also confirm that the smaller the cavity size, the more diffuse the transition, i.e. the larger the temperature range over which melting takes place [7]. The temperature at which the melting is initiated is seen to depend on the cavity size.

We have investigated whether the apparently diffuse melting transition is due to averaging the pressure over different cavities of the same size which individually show

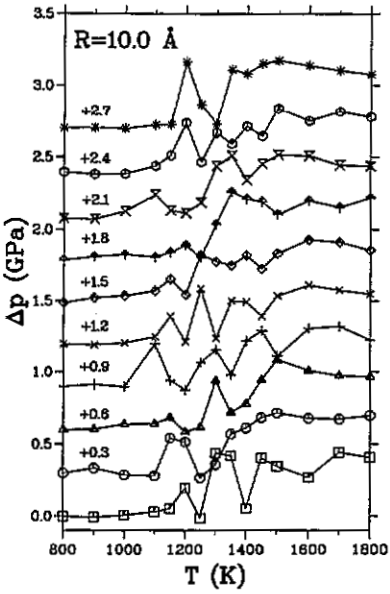

Figure 5. The excess pressure, defined as the difference between the observed pressure and a straight-line fit to the pressure below the onset of the melting transition, as a function of temperature for ten different runs in the small cavities. For clarity, the results for each run have been displaced vertically by an amount indicated (in GPa) for each of the curves in the figure.

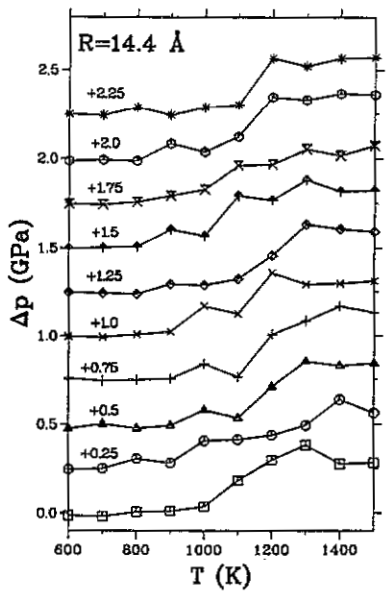

Figure 6. As for figure 5 except that these results are for the medium-sized cavities.

sharp phase transitions but at different temperatures, or if the phase transition is diffuse for each individual cavity. We did this by calculating excess pressure, ΔP, defined as the difference between the real pressure and the pressure obtained from a straight-line fit to the data below the melting transition (see figure 4). Figures 5 and 6 show our results for ΔP for cavities of effective radii 10 Å and 14.4 Å, respectively. The different curves show ΔP for the ten runs done for each system. Note that the results have been displaced vertically for clarity. These figures show very clearly that the phase transition is diffuse for each run and that there are strong fluctuations in the pressure which are greater for the smaller cavities.

3.3. Diffraction intensities

As shown in subsection 2.6 above, it is straightforward to calculate the diffraction intensities from the simulated positions of the rare-gas atoms in the cavities and to examine the transverse and longitudinal scans around a given diffraction peak, as shown in figure 1. The intensities for radial scans around the (111) peak are shown in figures 7 and 8. In all cases the results have been averaged over the ten runs done for each cavity size. Figure 7 gives our results for temperatures of 300 K, 900 K, 1100 K and 1300 K respectively for cavities with effective radius 14.4 Å and figure 8 gives results for cavities of effective radius 10.0 Å, 14.4 Å and 17.5 Å at 300 K and the temperature immediately above the melting region. An interesting feature, especially for the two smaller bubble sizes, is that even when the bubbles have melted there is

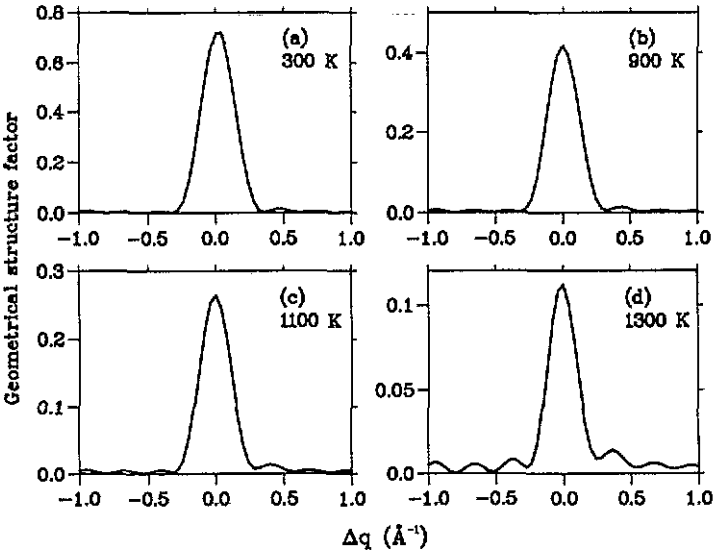

Figure 7. Radial scans of the geometrical structure factor around the (111) diffraction peak for medium-sized cavities (of effective radius 14.4 Å) at temperatures of 300 K (panel a), 900 K (panel b), 1100 K (panel c) and 1300 K (panel d). The scattering vector Δk for each point is given by equation (13) with $\delta_1 = \Delta q$ and a_{Kr}=5.62 Å.

apparently sufficient ordering to produce a weak diffraction peak.

The finite widths of the diffraction peaks arise from the finite number of atoms in each cavity and thermal disorder. The full width at half-maximum (FWHM) for the peaks in figure 7 is about 0.28 $Å^{-1}$ for temperatures 300 K, 900 K and 1100 K and about 0.22 $Å^{-1}$ at 1300 K. For figure 8, the FWHMs at 300 K are, respectively, about 0.39 $Å^{-1}$, 0.28 $Å^{-1}$ and 0.22 $Å^{-1}$. The FWHM for figure 8(*c*) agrees to within 10% with the width of 0.20 $Å^{-1}$ measured at 300 K by Andersen *et al* [13]. However, we do not observe the slight linear increase in FWHM with temperature seen in the experiments [13].

Calculations of transverse diffraction scans give results that are substantially different from the experimental results since the peak widths, like those for the radial scans, show very little variation with temperature. Thus, we do not reproduce the dramatic increase in the width of the transverse scans observed experimentally [13]. The implications of this finding are discussed below. We have not presented our data for the transverse peaks since they are very similar to the corresponding radial scans.

4. Discussion

4.1. Bubble pressures

A warning implicit in the results of section 3.2 is that deducing pressures inside bubbles from a bulk equation of state, even an accurate one, as is the normal practice in studies of bubbles in metals [16], is unlikely to give accurate results since we have demonstrated that the relationship between pressure and temperature depends on the cavity size. This observation casts doubt on much of the discussion of whether bubbles formed during ion implantation are over-pressurized, i.e. whether the pressure

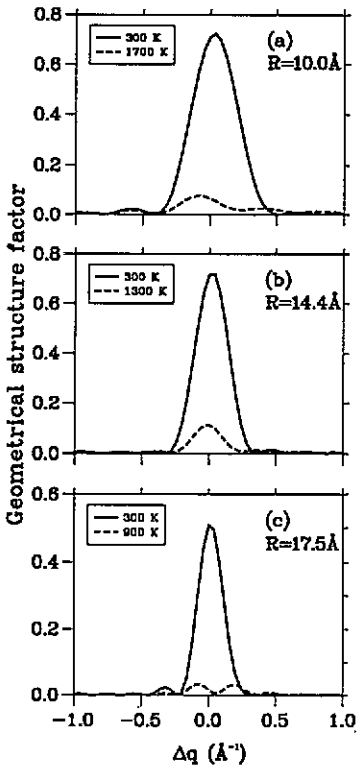

Figure 8. Radial scans of the geometrical structure factor around the ⟨111⟩ diffraction peak for (*a*) small, (*b*) medium- and (*c*) large-sized cavities. In each panel the solid and dashed lines correspond to temperature 300 K and a temperature immediately above the melting transition range, respectively. The scattering vector Δk for each point is given by equation (13) with $\delta_1 = \Delta q$ and a_{Kr}=5.62 Å.

of the gas is higher than the surface tension of the bubble, since the bubble pressure invariably has been estimated using a bulk equation of state [18, 20, 25].

4.2. The melting transition

One of the key results of this work is the observation of a broadened melting transition for the bubbles in analogy with that observed in simulations of isolated clusters [8, 10] and that the transition region between well-defined solid and fluid phases in some cases stretches over several hundred kelvin. Since the bubbles are embedded in a metal host it is straightforward to vary and monitor their temperature in experiments and the phase diagram can be examined by x-ray or electron diffraction. In particular, dark-field electron microscopy, which can monitor the diffraction intensity of *individual* bubbles [17, 20, 23], should be able to establish if there is a coexistence temperature range where bubbles are either solid or fluid and possibly determine if individual bubbles fluctuate between the two states—the observation of fluctuations obviously requires them to occur on a timescale compatible with the experiments. The pressure fluctuations shown in figures 5 and 6 may be between solid and liquid states; however, more work is required to establish this point.

There has been some discussion in the literature concerning 'superheating' effects in bubbles, i.e. whether the melting transition occurs at a higher temperature in a

bubble than for a bulk system with the same density [16, 22, 25]. In our results we see a clear size dependence of the melting transition—see section 3.2. However, the results also suggest why it is difficult to establish this effect experimentally. To establish whether superheating occurs one has to estimate the melting temperature for the equivalent bulk system. This has normally been done by employing a bulk equation of state to get a pressure which is then used to estimate the bulk melting temperature [16, 22, 25]. However, as discussed above, the use of a bulk equation of state is not appropriate for small bubbles. Furthermore, the broadened transition makes it difficult to identify a unique melting temperature experimentally.

We also find that even for a liquid bubble there is enough residual ordering to produce a solid-like diffraction peak, albeit of weak intensity. This result is consistent with the simulations of Jensen and Nieminen [27] of rare-gas atoms at a planar interface, who found that there were peaks in the gas density profiles for gas atoms close to the interface, even at temperatures where the bulk gas would be fluid. Their results and ours are related to the fact, proven by Finnis [41], that an arrangement of gas atoms with close-packed planes parallel to the cavity surface is energetically favourable compared to the condensation of the gas with loosely packed planes next to the metal. Jensen and Nieminen [27] conjectured that this ordering process might yield a solid-like diffraction pattern which is confirmed by the present results.

The recent Monte Carlo simulation study of surface melting for clusters confined to a spherical cavity by Chui [29] does indicate melting at the wall surfaces through calculations of the local structure factor. However, it is pointed out in that paper that this suppression of order is peculiar to small spherical systems. For flat walls, the author states that the local structure factor would be expected to increase near the walls and in that case that fluids would not nucleate at the surface, which would be more consistent with our observations.

Broughton [30] has simulated clusters coated with higher-melting-point material and found that such clusters have an enhanced stability against melting. It is hard to make a direct comparison with our results as the outer coating was not rigid (the cluster including its coating was confined to a region to maintain constant vapour pressure; however, that confinement did not interfere with the properties of the cluster) and the system size was an order of magnitude larger. However, it is interesting to see that in these simulations, as in ours, the interactions between the cluster and its coating or, in our case, between the cluster and cavity walls, are invoked to explain the superheating effects.

4.3. Diffraction from bubbles and misalignment

As described in section 3.3 we do not observe the dramatic increase in the width of transverse diffraction scans above 300 K detected in the x-ray diffraction measurements of Andersen *et al* [13]. In the original publication [13] this effect was interpreted as a loss of orientational alignment between the Kr in the bubbles and the Al host, possibly due to a roughening transition of the Al facets of the bubble which causes the cavity shapes to change from a truncated octahedron to approximately spherical. Bohr [26] has, as an alternative, recently suggested that the measurements may be explained by the presence of a fluid krypton layer between the krypton and the host metal. The results presented in section 3.3 for the atomic positions (figure 2) do not confirm this hypothesis and the fact that we do not see the transverse peak broadening in our simulations very strongly suggests that it cannot be due to movement of the Kr atoms alone, since the Kr motions should be described accurately by

the molecular dynamics method. Our results therefore support the earlier interpretation that the misalignment is due to rearrangement of the Al atoms at the cavity surface.

5. Conclusion

In this paper we have undertaken a computer simulation that for the first time has examined the melting of a cluster of particles in a confined geometry in detail. Specifically we have looked at the case of a rare-gas solid in a rigid cavity.

We find that the melting transition takes place over a finite temperature range due to the finite size of the system as has been observed earlier for isolated clusters. We have not found direct evidence for the coexistence of phases that has recently been explored in detail for isolated clusters [5,6], but observed pressure fluctuations that might signal oscillations between different phases.

We have shown that the equation of state is affected by the size of the cavity, in that the pressure differs significantly from that for a bulk system at the same density. It was also shown that the pressure calculated using the virial theorem (which is the standard procedure in molecular dynamics simulations) differs from that obtained directly from the force of the particles on the wall of the cavity when the range of the wall forces is non-zero.

Transverse and radial diffraction scans were calculated and compared with the experimental x-ray data of Andersen *et al* [13] for Kr bubbles in Al. Although we find good agreement for the full-width half-maxima (FWHM) for the radial scans (apart from not seeing a small linear increase with temperature), we do not see the very rapid increase in the FWHMs for the transverse peaks with temperature observed experimentally indicating that this effect is due to movement of the Al atoms on the cavity surface, e.g. in a roughening transition. Nor do we see clear evidence for the premelting at the surface of the rare-gas solid, suggested by Bohr [26].

We hope to extend the present work to a wider range of bubble sizes, bubbles shapes, and rare-gas densities and to investigate the behaviour in the melting transition region more closely. However, the results already obtained clearly demonstrate that rare-gas bubbles display the same type of melting behaviour as has attracted so much interest for isolated clusters and should hopefully inspire further experimental studies of the melting of rare-gas bubbles.

Acknowledgments

We would like to thank Anthony Clare for help with getting the simulation code running on the transputer array at the University of East Anglia, MF would like to thank the Science and Engineering Research Council and the Defence Research Agency, Malvern for a CASE studentship and KOJ would like to thank the Commission of the European Communities for a Research Grant under the Stimulation Action Scheme contract No SCI 0163.

References

[1] Tallon J L 1989 *Nature* 342 658

[2] Lee G C S and Low J C M 1989 *Phys. Rev.* B **39** 9302
[3] Martin C H and Singer S J 1991 *Phys. Rev.* B **44** 477
[4] Phillpot S R, Yip S and Wolf D 1989 *Comput. Phys.* Nov/Dec 20
[5] Jellinek J, Beck T L and Berry R S 1986 *J. Chem. Phys.* **84** 2783
[6] Davis H L, Jellinek J and Berry R S 1987 *J. Chem. Phys.* **86** 6456
[7] Imry Y 1980 *Phys. Rev.* B **21** 2042
[8] Berry R S and Wales D J 1989 *Phys. Rev. Lett.* **63** 1156
[9] Wales D J and Berry R S 1990 *J. Chem. Phys.* **92** 4473
[10] Labastie P and Whetten R L 1990 *Phys. Rev. Lett.* **65** 1567
[11] Hahn M Y and Whetten R L 1988 *Phys. Rev. Lett.* **61** 1190
[12] Fried L E and Mukamel S 1991 *Phys. Rev. Lett.* **66** 2340
[13] Andersen H H, Bohr J, Johansen A, Johnson E, Sarholt-Kristensen L and Surganov V 1987 *Phys. Rev. Lett.* **59** 1589
[14] Gråbaek L 1990 *PhD Thesis* University of Copenhagen (*Report* M-2868, Risø National Laboratory, Roskilde, Denmark)
[15] Bohr J and Gråbaek L 1991 *Fundamental Aspects of Inert Gases in Solids* ed S E Donnelly and J H Evans (Oxford: Plenum)
[16] Templier C 1991 *Fundamental Aspects of Inert Gases in Solids* ed S E Donnelly and J H Evans (Oxford: Plenum)
[17] Templier C, Garem H and Riviere J P 1986 *Phil. Mag.* A **53** 667
[18] vom Felde A, Fink J, Müller-Heinzerling Th, Pflüger J, Scheerer B, Linker G, Kaletta D 1984 *Phys. Rev. Lett.* **53** 922
[19] Evans J H and Mazey D J 1985 *J. Phys. F: Met. Phys.* **15** L1
[20] Mitchell D R G, Donnelly S E and Evans J H 1990 *Phil. Mag.* A **61** 531
[21] Jensen K O, Eldrup M, Pedersen N J, and Evans J H 1988 *J. Phys. F: Met. Phys.* **18** 1703
[22] Roussouw C J and Donnelly S E 1985 *Phys. Rev. Lett.* **55** 2960
[23] Donnelly S E and Roussouw C J 1986 *Nucl. Instrum. Methods* B **13** 485
[24] Birtcher R C and Jäger W 1985 *J. Nucl. Mater.* **135** 274
[25] Faraci G, La Rosa S, Penisi A R, Mobilio S and Tourillon G 1991 *Phys. Rev.* B **43** 9962
[26] Bohr J 1991 *Z. Phys.* D **20** 215
[27] Jensen K O and Nieminen R M 1987 *Phys. Rev.* B **36** 8219
[28] Bug A L R 1989 *Int. J. Thermodyn.* **10** 469
[29] Chui S T 1991 *Phys. Rev.* B **43** 11523
[30] Broughton J 1991 *Phys. Rev. Lett.* **67** 2990
[31] Lucas A A 1984 *Physica* B **127** 225
[32] Ashcroft N W and Mermin N D 1976 *Solid State Physics* (New York: Holt, Reinhart and Winston)
[33] Manninen M, Nørskov J K, Puska M J, Umrigar C 1984 *Phys. Rev.* B **29** 2314
[34] Brown A P, Walker A B and West R N 1987 *J. Phys. F: Met. Phys.* **17** 2491
[35] Siska P E, Parson J M, Schaafer T P and Lee Y T 1971 *J. Chem. Phys.* **55** 5762
[36] Ross M, Mao H, Bell P M and Xu J A 1986 *J. Chem. Phys.* **85** 1028
[37] Kartunen V, Ignatius J, Keinonen J and Nieminen R M 1989 *J. Phys.: Condens. Matter* **1** 4885
[38] Allen M and Tildesley D 1989 *Computer Simulation of Liquids* (Oxford: Oxford University Press)
[39] Powles J G, Rickayzen G and Williams M L 1985 *J. Chem. Phys.* **83** 293
[40] Hirschfelder J O, Curtis C F and Bird R B 1964 *Molecular Theory of Gases and Liquids* (New York: Wiley)
[41] Finnis M W 1987 *Acta Metall.* **35** 2543